On the formation of dwarf galaxies and stellar haloes

J. I. Read,[1][*] A. P. Pontzen[2] and M. Viel[2,3]

[1]*Institute of Theoretical Physics, University of Zürich, Wintherurestrasse 190, 8057 Zurich, Switzerland*
[2]*Institute of Astronomy, Cambridge University, Madingley Road, Cambridge CB3 OHA*
[3]*INAF - Osservatorio Astronomico di Trieste, Via G.B. Tiepolo 11, I-34131 Trieste, Italy*

ABSTRACT

Using analytic arguments and a suite of very high resolution ($\sim 10^3$ M$_\odot$ per particle) cosmological hydrodynamical simulations, we argue that high-redshift, $z \sim 10$, $M \sim 10^8$ M$_\odot$ haloes, form the smallest 'baryonic building block' (BBB) for galaxy formation. These haloes are just massive enough to efficiently form stars through atomic line cooling and to hold on to their gas in the presence of supernova (SN) winds and reionization. These combined effects, in particular that of the SN feedback, create a sharp transition: over the mass range 3–10×10^7 M$_\odot$, the BBBs drop two orders of magnitude in stellar mass. Below $\sim 2 \times 10^7$ M$_\odot$, galaxies will be dark with almost no stars and no gas. Above this scale is the smallest unit of galaxy formation: the BBB.

We show that the BBBs have stellar distributions which are spheroidal, of low rotational velocity, old and metal poor: they resemble the dwarf spheroidal galaxies (dSphs) of the Local Group (LG). Unlike the LG dSphs, however, they contain significant gas fractions. We connect these high-redshift BBBs to the smallest dwarf galaxies observed at $z = 0$ using linear theory. A small fraction (~ 100) of these gas-rich BBBs at high redshift fall in to a galaxy the size of the Milky Way (MW). We suggest that 10 per cent of these survive to become the observed LG dwarf galaxies at the present epoch. This is consistent with recent numerical estimates. Those infalling haloes on benign orbits which keep them far away from the MW or Andromeda manage to retain their gas and slowly form stars – these become the smallest dwarf irregular galaxies; those on more severe orbits lose their gas faster than they can form stars and become the dwarf spheroidals. The remaining 90 per cent of the BBBs will be accreted. We show that this gives a metallicity and total stellar mass consistent with the MW old stellar halo.

Key words: galaxies: haloes – galaxies: kinematics and dynamics – cosmology: theory.

1 INTRODUCTION

The Local Group (LG) of galaxies provide a unique test-bed for galaxy formation theories and cosmology. Their close proximity allows individual stars to be resolved giving accurate kinematics, stellar populations and star formation histories (see e.g. Kleyna et al. 2001; Dolphin 2002); their spatial distribution can be compared with cosmological predictions to give useful constraints (Moore et al. 2006); and their large mass-to-light ratios can be used, through dynamical modelling, to place constraints on the nature of dark matter (Kleyna et al. 2001).

The LG dwarf galaxies are usually split into three types: dwarf spheroidal galaxies (dSphs), which typically have old stellar populations, are spheroidal in morphology, lie close to their host

galaxy[1] and are devoid of H I gas; dwarf irregular galaxies (dIrrs), which have younger stellar populations, irregular morphology, lie further away from their host galaxy and contain significant H I gas; and the transition galaxies, which are in between the dSph and dIrr types (Mateo 1998).

In our current 'vanilla' cosmological paradigm (ΛCDM – cold dark matter with a cosmological constant), all structure forms from the successive mergers of smaller substructures (White & Rees 1978). While this theory has been tremendously successful on scales larger than ~ 1 Mpc, on smaller scales it has fared less well (see e.g. D'Onghia & Lake 2004). A now long-standing puzzle is the 'missing satellites' problem: there appears to be an order of magnitude fewer satellite galaxies in the LG than would naively be predicted from the mass function of dark matter haloes (see e.g.

---

[1]We use the terminology 'host galaxy' throughout this paper to refer to either the Milky Way (MW) or Andromeda (M31) depending on which of these is closer to the satellite being discussed.

[*]E-mail: justin@physik.unizh.ch

Kauffmann, White & Guiderdoni 1993; Klypin et al. 1999). A number of solutions to this puzzle have been presented; the two main threads being either to alter the nature of dark matter (Avila-Reese et al. 2001; Bode, Ostriker & Turok 2001), or to invoke some form of feedback from supernova (SN) explosions (see e.g. Larson 1974; Efstathiou 2000), or photoevaporation (see e.g. Quinn, Katz & Efstathiou 1996; Barkana & Loeb 1999). In the feedback scenario, one might naively expect only the most-massive substructure satellites, with the deepest potential wells, to form stars and remain visible in the LG at the present epoch (Stoehr et al. 2002). However, this presents a problem since the most-massive substructure dark matter haloes predicted by ΛCDM models have central stellar velocity dispersions which are factors of 2–3 larger than those observed in the LG satellites, even after extreme tidal stripping of shocking of these haloes (Hayashi et al. 2003; Kazantzidis et al. 2004; Read et al. 2006a).

An alternative view is that the LG satellites are fossil galaxies left over from reionization[2] (Bullock, Kravtsov & Weinberg 2000, 2001; Benson et al. 2002; Kravtsov, Gnedin & Klypin 2004; Susa & Umemura 2004; Kawata et al. 2005; Ricotti & Gnedin 2005; Gnedin & Kravtsov 2006). In this scenario, only those rare overdense peaks which collapse before redshift $z \sim 10$ (the epoch of reionization) and achieve a potential well deep enough to form stars remain visible at the present epoch; the remaining satellite galaxies have star formation quenched by the background UV flux from reionization. In this model it is not the most-massive substructure haloes at $z = 0$ which are the LG satellites, but rather the *survivors* from haloes which form stars at $z \sim 10$. There is observational evidence for such a scenario, both indirectly from high-redshift quasar absorption spectra (Wyithe & Loeb 2006), and from the star formation histories of LG dIrrs, which show a strong suppression in star formation up to $z \sim 1$ (Skillman 2005).

While this general model has been investigated by a number of authors in the literature, there are significant differences in the details. Kravtsov et al. (2004) argued that only a few of the LG satellites are genuine fossils; the majority were significantly more massive in the past, formed most of their stars after reionization (at $z \sim 3$), and then subsequently lost their mass through tidal stripping and shocking. They found that the central velocity dispersions can be sufficiently lowered in their model once satellite–satellite interactions are taken into account alongside stripping and shocking from the MW or Andromeda (M31). This model complements the 'tidal model' proposed by Mayer et al. (2001a) and Mayer et al. (2001b) to explain the distance–morphology relation between dSphs and dIrrs. In these two papers, it is suggested that all the LG satellite galaxies started out looking more like the dIrrs with a disc-like morphology. Those satellites on orbits which brought them close to the MW or M31 then formed induced bars which buckled leaving a spheroidal remnant: a dSph.

Ricotti & Gnedin (2005) and Gnedin & Kravtsov (2006) focused on the pure fossils left over from reionization. They presented a detailed cosmological model which includes radiative transfer and molecular cooling from H_2. These new key ingredients allowed

them to study star formation in mini haloes with virial temperatures $T < 10^4$ K – the temperature at which hydrogen starts to become collisionally ionized. They found, contrary to previous studies, that such minihaloes can cool efficiently and form stars. They posited that such haloes could then (if they survive) be the progenitors of dSphs in the LG. They require more massive haloes to then become the dIrrs. However, they do naturally recover the spheroidal morphology, low gas fractions, low rotational velocity and old stellar populations observed in the LG dSphs (see e.g. Mateo 1998), without recourse to any tidal transformations.

Ricotti & Gnedin (2005) and Gnedin & Kravtsov (2006) study in detail the effects of photoionizing feedback from star formation. They also include a heating term due to feedback from SNe. However, they do not include the effects of feedback from SN winds. In this paper, we implement and test the effect of both kinds of feedback: a heating term that inhibits star formation, and galactic wind driven by SN explosions. This is a key difference in the work we present here. Observationally, we can see that SN winds are driven in galaxies undergoing a phase of star formation and that such winds are important, especially on the scale of dwarf galaxies (see e.g. Ott, Walter & Brinks 2005). Theoretically, Mac Low & Ferrara (1999) and Marcolini, D'Ercole & Brighenti (2006) have shown that there is a transition scale at about $M_{crit} \sim 10^7$–10^8 M$_\odot$ below which dwarf galaxies efficiently lose their gas from SN winds[3]; while Dekel & Silk (1986) and Dekel & Woo (2003) demonstrated that SN feedback could account for the global scaling relations of the LG dwarfs.

In this paper, we use a suite of very high resolution cosmological hydrodynamical simulations, which include gas cooling, star formation, feedback from SNe, galactic winds and reionization, to study a new model for the formation of the LG dwarf galaxies. We do not include the effects of the detailed radiative transfer and cooling physics required to model star formation in minihaloes with mass $M \lesssim 10^7$ M$_\odot$, since we are interested primarily in haloes more massive than this. We suggest that the smallest dwarf galaxies of the LG share a common progenitor: rare, $\sim 3\,\sigma$, $\gtrsim 10^8$ M$_\odot$, dark matter haloes at $z \sim 10$. These haloes are just massive enough to efficiently form stars through atomic line cooling and to hold on to their gas in the presence of SN winds and reionization. As a result, they are the smallest 'baryonic building block' (BBB) available for galaxy formation.

Some of these gas-rich early-forming galaxies fall in late to the LG and survive as dwarf galaxies. Those infalling haloes on benign orbits which keep them far away from the MW or M31 manage to retain their gas and slowly form stars – these become the dIrrs; those on more severe orbits lose their gas faster than they can form stars and become the dSphs. This suggests that the dIrrs should also have an old extended spheroidal component of stars: a stellar halo. There is increasing observational evidence that this is indeed the case (Minniti & Zijlstra 1996; Aparicio, Tikhonov & Karachentsev 2000; Minniti et al. 2003; and see Vaduvescu et al. 2005 for a study of dIrrs outside the LG). It also suggests that the star formation histories of the LG dwarfs should all show an early, pre-reionization burst of star formation. This also appears to be the case (see e.g. Hernandez, Gilmore & Valls-Gabaud 2000; Dolphin 2002).

The idea of a smallest building block has a long history in the literature. Hoyle (1953) pointed out that gas cooling becomes efficient

---

[2]The epoch of reionization is caused by ultraviolet (UV) flux emitted by the first-forming massive stars. Throughout this paper, we suggest that reionization occurred at $z \sim 10$. Observationally, there are two bounds on this epoch. The old *Wilkinson Microwave Anisotropy Probe* (*WMAP*) satellite data favour larger redshifts (Spergel et al. 2003); the data from quasar absorption spectra favour smaller redshifts (Fan et al. 2005; but see also Bunker et al. 2006); the new *WMAP* data favour our chosen redshift (Spergel et al. 2006).

[3]We note, however, that this conclusion is degenerate with the mechanical luminosity in the wind. For the mean plausible range, efficient mass loss occurs at $\sim 10^7$ M$_\odot$.

for ionized hydrogen at 10^4 K; Peebles & Dicke (1968) presented a model with a smallest mass block of $10^5 \, M_\odot$ for star formation in the context of globular clusters; Peebles (1984) updated this argument to include dark matter and showed that the relevant mass was $\sim 10^8 \, M_\odot$, as suggested here; and, from an observational point of view, Searle & Zinn (1978) showed that the galactic globular cluster abundances are not correlated with distance – a result which has led to the hierarchical merging model being currently favoured over the then-popular model of monolithic collapse (Eggen, Lynden-Bell & Sandage 1962). Here, we take the next logical step by investigating the morphology and kinematics of the stars, gas and dark matter in these high-redshift BBBs, and making a link to the smallest galaxies observed in the LG at the present epoch.

To test our model, we use a small box size of 1 Mpc and stop the simulation at $z = 10$ (to avoid simulations becoming non-linear on the scale of the box). With such a small box size, we achieve an unprecedented mass resolution of $\sim 10^3 \, M_\odot$ per particle. This allows us to accurately track the kinematics and morphology of galaxies of total mass $M \sim 10^8 \, M_\odot$ and compare our results with observations from the LG dwarfs. Ideally, one would like to use a larger box and evolve all the way to redshift $z = 0$. However, this is not technically feasible for a mass resolution of $\sim 10^3 \, M_\odot$ per particle, at the present time. Instead, we have to compromise by stopping at redshift $z = 10$ and making the link to redshift $z = 0$ using a mixture of linear theory arguments (Section 2) and results from other studies in the literature (Mayer et al. 2005; Moore et al. 2006).

This paper is organized as follows. In Section 2, we present some theoretical motivation for our model. In Section 3, we describe the simulations. We used a control simulation with only dark matter, and five other simulations which explore the effect of the star formation prescription and SN winds of varying strength. All simulations were run with identical initial phase-space distributions. In Section 4, we describe the results from our suite of high-resolution simulations. In Section 5, we discuss our results in the context of recent observations. Finally, in Section 6, we present our conclusions.

2 THEORETICAL MOTIVATION: THE 'BARYONIC BUILDING BLOCK'

The mass scale, $M_{\rm crit} \sim 10^8 \, M_\odot$, is interesting. First, it corresponds to the mass below which a galaxy cannot retain its gas in the presence of SN winds (Mac Low & Ferrara 1999; Marcolini et al. 2006[4]). Secondly, the virial temperature of haloes at a given redshift, $T_{\rm v}$, is given by (Peacock 1999):

$$T_{\rm V}/{\rm K} = 10^{5.1} \left(\frac{M}{10^{12} \, M_\odot} \right)^{2/3} (f_{\rm c} \Omega h^2)^{1/3} (1 + z), \tag{1}$$

where M is the mass of the halo; z is the redshift; $h = 0.72$ is the dimensionless Hubble parameter at the present epoch; $\Omega = \Omega(z)$ is the ratio of the halo density to the critical density; and $f_{\rm c}$ is the density enhancement of the collapsing halo with respect to the background. Working at high redshift ($z = 10$) has the advantage that $\Omega \simeq 1$, irrespective of the cosmological model. Spherical top-hat collapse then gives $f_{\rm c} \simeq 178$ at virialization (Peacock 1999).

The temperature, $T_{\rm v} = 10^4$ K, is the temperature scale at which hydrogen starts to collisionally ionize. This allows for efficient atomic line cooling. Below this temperature, hydrogen can only

[4]In fact, Marcolini et al. (2006) found that $M_{\rm crit} \sim 2 \times 10^7 \, M_\odot$ as a result of metal cooling. This slightly lower bound does not affect our argument.
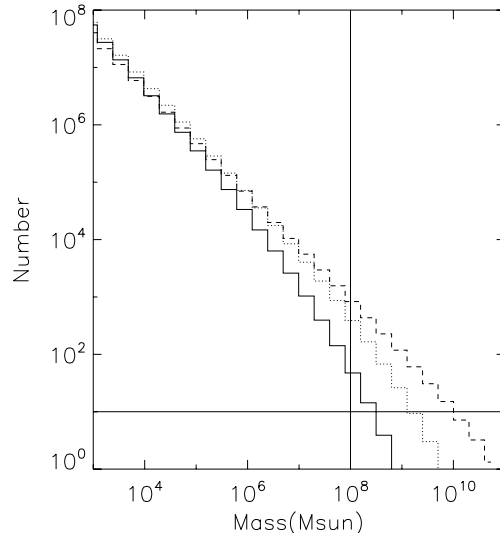

Figure 1. The number of haloes, N, formed up to redshift $z = 15$, 10 and 5 (solid, dotted and dashed lines, respectively), in a given mass range which are likely to have fallen into a larger halo of mass $M_0 = 2 \times 10^{12} \, M_\odot$ at $z_0 = 0$. Overplotted are the number of dSphs currently observed around the MW (horizontal line) and the mass scale $M_{\rm crit}$ (vertical line).

cool through radiative emission from H_2 roto-vibrational transitions, which is very inefficient by comparison (Le Bourlot, Pineau des Forêts & Flower 1999). Using $T_{\rm v} = 10^4$ K and $z = 10$ gives $M = 6.4 \times 10^7 \, M_\odot \simeq M_{\rm crit}$. Thus, just before the epoch of reionization ($z = 10$), haloes which reach a virial temperature of $T_{\rm v} = 10^4$ K and can efficiently form stars are those of mass $M_{\rm crit}$.

Thirdly, the Extended Press–Schechter (EPS) scheme (Lacey & Cole 1993) can be used to calculate the mean number of haloes of a given mass and redshift, M, z, which fall into a larger halo of given mass and redshift, M_0, z_0:

$$\frac{{\rm d}N}{{\rm d}\ln M} = \sqrt{\frac{2}{\pi}} M_0 \sigma_0(M) \frac{D}{S^{3/2}} \exp\left(-\frac{D^2}{2S} \right) \left| \frac{{\rm d}\sigma_0(M)}{{\rm d}M} \right|, \tag{2}$$

where $D = \delta_{\rm c}[D(z)^{-1} - D(z_0)^{-1}]$; $S = \sigma_0^2(M) - \sigma_0^2(M_0)$; $\sigma_0^2(M)$ is the variance of the linear power spectrum at $z = 0$ smoothed with a top-hat filter of mass M; $\delta_{\rm c}$ is the critical overdensity for spherical collapse; and $D(z)$ is the growth factor which depends on the cosmology.[5]

Integrating equation (2) allows us to solve for the number of haloes, N, formed from the beginning of the universe *up to* some redshift z, in a given mass range, which are likely to have fallen into a larger halo of mass $M_0 = 2 \times 10^{12} \, M_\odot$ (approximately equal to the mass of the MW, Wilkinson & Evans 1999) at $z_0 = 0$. This is what we plot in Fig. 1 for $z = 15$, 10 and 5 (solid, dotted and dashed lines, respectively). The formation redshift for these haloes, z, then corresponds to the epoch of reionization, before which the LG dwarf spheroidals could form stars. Overplotted are the number

[5]Usually it is stated that $\delta_{\rm c} = 1.69$, but this is only true for a universe with $\Omega_{\rm m} = 1$, where $\Omega_{\rm m}$ is the ratio of the matter density of the universe to the critical density required for closure. Here, we calculate $\delta_{\rm c}$ and $D(z)$ correctly (numerically) for a ΛCDM cosmology in which $\Omega_{\rm m} + \Omega_\Lambda = 1$, where Ω_Λ is the ratio of the dark energy density to the critical density, or the 'cosmological constant'. The relevant equations for this are given in Eisenstein & Hu (1999). The cosmological parameters we use are given in Section 3.

of dSphs currently observed around the MW (horizontal line) and the mass scale M_{crit} (vertical line). For early reionization $z \gtrsim 10$, such as that favoured by the *WMAP* data (Spergel et al. 2003), the total number of satellites with mass 10^7–10^8 M$_\odot$ is of the order of 100. This is an order of magnitude greater than the observed number in the LG. However, it is the number which will be *accreted* by an MW-sized halo, not the number which survives as satellite haloes at $z = 0$. Moore et al. (2006) have recently shown that only ~10 per cent survive, giving the correct order of magnitude of satellites around the MW. A final encouraging point is that the total stellar mass in the accreted satellites is then $\sim10^8$ M$_\odot$, which is the mass of the MW old stellar halo (Binney & Merrifield 1998). Note that, the above requires early reionization. If reionization is found to occur much later ($z \sim 5$), this would rule out our model. Turning this around, we tentatively suggest that the LG dwarf galaxies' number and distribution can constrain the epoch of reionization.

$M_{crit} \sim 10^8$ M$_\odot$ appears to be a critical mass scale at which gas cooling becomes efficient so that star formation can occur; and at which the potential well is just deep enough to hold on to the remaining gas left over from star formation in the presence of SN winds. The number of surviving subhaloes of this mass formed at $z \sim 10$ which fall into an MW-sized halo at $z = 0$ is consistent with the observed number of LG satellites, while observations of the LG and nearby dwarfs suggest masses of the order of 10^8 M$_\odot$ (see Fig. 7). These facts, combined with the mounting evidence for old stellar haloes in the dIrrs, and star formation histories which show pre-reionization bursts, form the main motivation for investigating our model in more detail.

3 HYDRODYNAMICAL SIMULATIONS

We ran hydrodynamical simulations using the new version of the parallel TreeSPH code GADGET-2 (Springel, Yoshida & White 2001; Springel 2005). GADGET-2 was used in its TreePM mode which speeds up the calculation of long-range gravitational forces considerably. The simulations were performed with periodic boundary conditions with an equal number of dark matter and gas particles and used the conservative 'entropy-formulation' of smoothed particle hydrodynamics (SPH) proposed by Springel & Hernquist (2002). Radiative cooling and heating processes were followed using an implementation similar to that of Katz, Weinberg & Hernquist (1996) for a primordial mix of hydrogen and helium. We assumed a mean UV background produced by quasars as given by Haardt & Madau (1996), and we switched the background on at high redshift in order to have H I reionization at $z \sim 13$. Such a treatment for the reionization is quite crude: we simply stretched the epoch of reionization and switched on a uniform background at $z \sim 13$, instead of $z \sim 6$. However, even if the details are incorrect (to correctly follow reionization, one would need a radiative transfer code), we obtain the behaviour we expect, that is, a jump in the gas temperature that brings most of the gas elements to $T \sim 10^4$ K. Note also that, the effect of reionization only really enters at the very end of our simulations and serves only to inhibit further star formation.

We used 2×448^3 dark matter and gas particles in a comoving 1 Mpc h^{-1} box. The simulations were all started at $z = 199$ and we have stored 19 redshift outputs for each run, mainly in the redshift range $10 < z < 30$. The initial gas temperature was $T = 546$ K, and 40 ± 2 SPH neighbours were used to compute physical quantities. The gravitational softening was set to 0.055 h^{-1} kpc in comoving units for all particles.

Our fiducial model was a 'concordance' ΛCDM model with $\Omega_{0m} = 0.26$, $\Omega_{0\Lambda} = 0.74$, $\Omega_{0b} = 0.0463$ and $H_0 = 72 \, \mathrm{km \, s^{-1} \, Mpc^{-1}}$,

$n = 1$ and $\sigma_8 = 0.9$.[6] This model is in agreement with most of the observations including the parameters inferred by the *WMAP* team in their first year data release and the recent results of the Lyman α forest community (Spergel et al. 2003; Viel, Haehnelt & Springel 2004; Seljak et al. 2005). The CDM transfer functions of all models have been taken from Eisenstein & Hu (1999).

We note that the new three-year data release by the *WMAP* team (Spergel et al. 2006) pointed to smaller values for the spectral index and σ_8, while the new reionization redshift is perfectly consistent with that chosen in our simulations. These new values should not have a large impact on the internal structure of the haloes we investigate in this paper, but the lower σ_8 will affect the statistics of such haloes. We note that, when combined with data from the Lyman α forest, the *WMAP* three-year data release favours higher values of σ_8, similar to those we use here (Viel, Haehnelt & Lewis 2006; Seljak, Slosar & McDonald 2006). As such we felt it would be premature to re-run our simulations with lower σ_8.

We ran six different simulations in total. One with dark matter only was run as a control simulation and is only briefly mentioned. The other five investigate different star formation prescriptions and wind strengths. In all cases, we started with identical initial phase-space distributions. We used two different star formation recipes. The first (A) was a very simplified prescription based only on a density and temperature cut. All gas is turned into stars when the overdensity, $\delta > 1000$ and the temperature, $T < 10^5$ K. This simple prescription does not track or calculate metallicities for the stars and gas. The second (B) was more physically motivated and modelled a subparticle multiphase medium, including SN feedback. This SN feedback is represented by a local heating term near star-forming regions and does not drive a global galactic wind. This model is described in detail in Springel & Hernquist (2003). We used the 'simplified', rather than the 'explicit' mode of star formation. We list all the parameters for both prescriptions in Table 1.

In addition to each star formation prescription, we investigated the effect of adding a SN-driven galactic wind. The wind model we use is described in detail in Springel & Hernquist (2003). We assumed that the galaxy mass loss rate that goes into a wind, $\dot{M}_w$, is proportional to the star formation rate itself:

$$\dot{M}_w = \eta \dot{M}_\star, \tag{3}$$

where η is a coefficient of the order of unity. Moreover, we assumed that the wind carries a fixed fraction χ of the SN energy. Equating the kinetic energy in the wind with the energy input by SNe,

$$\frac{1}{2}\dot{M}_w v_w^2 = \chi \epsilon_{SN} \dot{M}_\star, \tag{4}$$

we obtain the wind's initial velocity as

$$v_w = \sqrt{\frac{2\chi \epsilon_{SN}}{\eta}}, \tag{5}$$

---

[6] We use the common nomenclature where Ω_{0m}, $\Omega_{0\Lambda}$ and Ω_{0b} are the ratio of the density of the universe in matter, dark energy and baryons, respectively, at redshift, $z = 0$, to the critical density required for closure; H_0 is Hubble's constant at $z = 0$; n is the *initial* spectral index of initial matter fluctuations (1 corresponds to scale-invariance); and σ_8 is the amplitude normalization of matter fluctuations at $z = 0$: the rms density variation of the universe smoothed with a top-hat filter of radius 8 h^{-1} Mpc ($h = 0.72$ is the dimensionless Hubble parameter) at $z = 0$. Note that one should be cautious of this definition of σ_8 since it implicitly assumes that linear theory can connect the initial and $z = 0$ amplitude of fluctuations. On scales as large as h^{-1} Mpc at $z = 0$ this is usually ok, but non-linearities can certainly affect the expected peculiar velocities on these scales (see e.g. Peel 2006).

Table 1. Free parameters in the model and their observational constraints. Parameters are split into those which govern star formation (above) and those controlling the SN winds (below). The columns from left-hand to right-hand side give the star formation prescription (SFP), free model parameters, a brief description of the free parameter, and observational constraints on that parameter. The metallicity is not constrained by independent observations (observations not of dwarf galaxies). We use a value based on Theuns et al. (2002). They found $p = 3$ provides the best fit to the metallicity of the IGM at $z = 3$.

SFP	Free parameter	Description	Constraint
A	$\delta_c = 1000$	Critical overdensity for star formation	Unconstrained
A	$T_c = 10^5 \, \mathrm{K}$	Critical temperature for star formation	Unconstrained
B	$\beta = 0.1$	Mass fraction in stars $>8 \, \mathrm{M}_\odot$	Salpeter IMF
B	$t_0^* = 2.1 \, \mathrm{Gyr}$	Star formation time	Fit to the Kennicutt (1989) law
B	$p = 3 \, \mathrm{Z}_\odot$	Metallicity yield	Based on Theuns et al. (2002); poorly constrained
A/B	$\epsilon_{SN} = 10^{44} \, \mathrm{J}$	SN energy	Canonical value
A/B	$\eta = 2$	Wind mass loss rate	Observed (Martin 1999; Ott et al. 2005)
A/B	$v_{wind} = 0, 221.8$ and $483.6 \, \mathrm{km \, s^{-1}}$	Wind speed	Observed (Martin 1999; Ott et al. 2005)

with $\epsilon_{SN} = 4 \times 10^{45} \, \mathrm{erg \, M_\odot^{-1}}$, which is the average expected value from the SN explosions' energy release ($10^{51} \, \mathrm{erg}$). These parametrizations and the chosen values are mainly motivated by observations of starburst-driven galactic winds in the local Universe (e.g. Martin 1999; Ott et al. 2005).

We investigated each star formation prescription without winds (no wind A/B: NWA/B), and with winds of varying strength (weak wind A/B: WWA/B; strong wind A: SWA). The 'weak wind' (WW) and 'strong wind' (SW) runs had $\chi = 0.25$ and 1 and $\eta \equiv 2$ which resulted in an average speed of the wind of 221.8 and 483.6 km s^{-1}, respectively.

Although the effects of galactic winds at $z > 10$ are not clear and very difficult to quantify, we note that the feedback prescription used here predicts a global star formation history and an intergalactic medium (IGM) metal enrichment at $z = 3$ that are in good agreement with observations (Springel & Hernquist 2002). The effect of feedback by galactic winds on the IGM structures that surround galaxies at $z \sim 3$ is extremely uncertain (e.g. Theuns et al. 2002; Adelberger et al. 2003, 2005; Desjacques et al. 2004; Rauch et al. 2005), but we stress that the values of the speed of the wind, used in the feedback simulations (although at much higher redshift), are in rough agreement with local observations (Ott et al. 2005).

However, some caution is appropriate. There can be many free unconstrained parameters and, with fine tuning, one wonders if any set of observations could eventually be reproduced. In an attempt to assuage these fears and give more confidence to the simulations, we have briefly summarized all the free parameters in the model and how they have been constrained in Table 1; the constraints are essentially the same as those outlined in Springel & Hernquist (2002). The simple star formation prescription (A) is not well motivated by observations, but serves to investigate the dependence of our results on the unknown star formation recipe. For prescription (B), there are a number of free parameters. However, note that all these are constrained by independent observations except for the metallicity yield. We have not fine-tuned any of the parameters to achieve a particular result. This means that our model should produce believable physical results, with the exception of the absolute value (not the spread) of the metallicity. The absolute metallicity has been 'tuned' to fit the metallicity of the IGM at $z = 3$ (Theuns et al. 2002). However, for dwarf galaxies forming at $z = 10$, it could conceivably be quite different. We comment further on this in Section 4.4.

It is worth briefly noting some points of contention about the observations we use to constrain our model parameters. First, we assume a Salpeter initial mass function (IMF) of stars. However, it is difficult to measure the massive end of the stellar mass function

since these stars are so short lived. Yet this is the region of most interest for determining the strength of the SN feedback and winds. Certainly the first-forming stars would appear, in theoretical models, to have an IMF biased towards the high-mass end (Abel et al. 1998). Secondly, our wind model posits that winds are driven during any period of star formation, even during relatively quiescent periods (recall that $\dot{M}_w = \eta \dot{M}_\star$). Alternatives link winds only to starbursts which are short lived (Mac Low & Ferrara 1999). There is, then, a potential danger in linking observations of starbursting dwarfs with our more continuous wind model. However, in the simulations, the majority of the stars form over a short time-scale (see Section 4), so this should not be too great a concern.

The galaxies were extracted from the simulation volume using a Friends-of-Friends algorithm with linking length $l = 0.2$. We follow the iterative method of Porciani, Dekel & Hoffman (2002) to ensure that the extracted haloes are bound. At each stage the total energy of each particle is calculated. Particles which do not appear to be bound are excluded from the potential calculation in the next stage. The momentum centre of the bound group is also calculated; this means particles excluded at one stage may later re-enter the calculation. We perform our analysis using only the bound component, although our tests show that the difference in profiles obtained is not significant.

4 RESULTS

In this section, we present the results from our suite of hydrodynamical simulations. Recall that we have to stop these simulations at $z = 10$ due to our small box size. This makes connecting the galaxies we form in our simulations to galaxies observed at $z = 0$ difficult. The most-massive galaxies we form have mass $\sim 10^8 \, \mathrm{M}_\odot$. From the linear theory arguments given in Section 2, we expect that ~ 100 of these galaxies will be accreted on to a galaxy the size of the MW. Most will be accreted; 10 per cent will survive, as shown by Moore et al. (2006). We can expect many of these survivors at $z = 0$ to look very different from the galaxies we form at $z = 10$. However, the smallest gas-poor galaxies in the LG at $z = 0$ (the dSphs) are known to have very old stellar populations. As such, we can constrain our model by comparing the stellar distributions and metallicity of our most-massive galaxies with data from the dSphs of the LG at the present epoch (see Sections 4.2 and 4.4). The connection to the dIrrs will be more tentative, but we attempt this in Section 4.5.

4.1 Overview

Fig. 2 shows the projected dark matter, star and gas densities for the second most-massive halo in the no wind A (NWA), no wind B
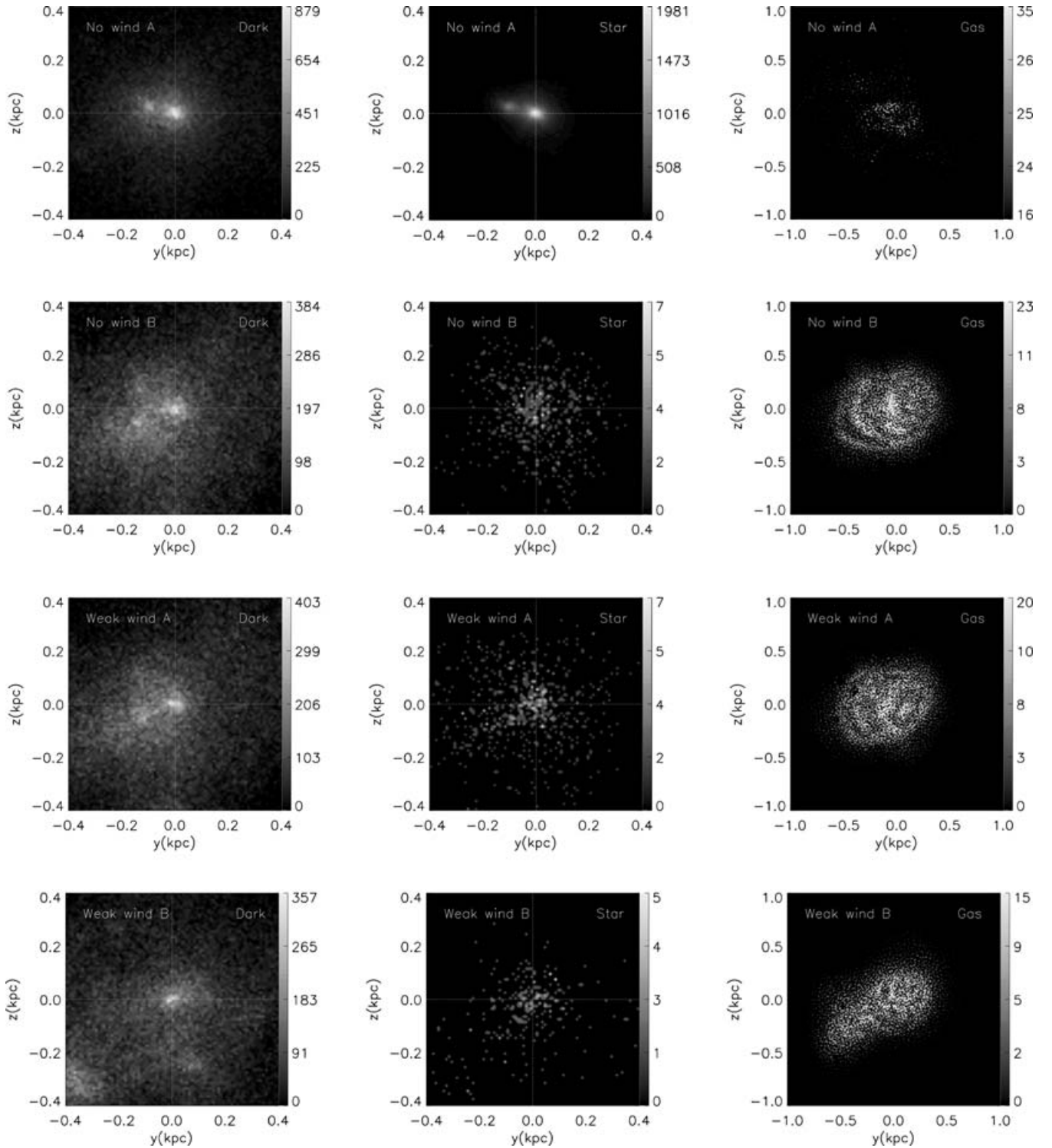
Figure 2. Projected density for the dark matter (left-hand panel), stars (middle panel) and gas (right-hand panel), for (from top to bottom panel) the NWA, NWB, WWA and WWB simulations; second most-massive halo. The gas density is for a thin slice of width 0.1 kpc about the *x*-axis. The contour bars show density in units of $10^6 \, M_\odot \, \text{kpc}^{-3}$ in all cases, except the NW gas density, which is in units of $10^4 \, M_\odot \, \text{kpc}^{-3}$. Note that the gas is more extended and less concentrated than the stars and dark matter and for this reason the gas is plotted on a different scale. All simulations were run with identical initial phase-space distributions. This means that the above haloes are identical apart from their star formation and feedback prescriptions. The key thing to note is that without any SN feedback (NWA) there is significant star formation; all the most-massive substructures and the central halo have bound stars. In contrast, with SN feedback, the NWB, WWA and WWB simulations are similar: there is very little star formation and significant remaining gas. The form of the feedback is not critical. NWB uses a heating term for the SN feedback; WWA uses a SN-driven galactic wind; WWB uses both. Since NWB and WWA are so similar, we show only results for the NWB simulation from hereon.

(NWB), weak wind A (WWA) and weak wind B (WWB) simulations. We do not show the results for the SW simulations since these are identical to the WW runs: the wind strength, for the plausible range of observed wind speeds, is not an important factor in our wind model. We present results for the SWA simulation alongside the others in Section 4.5.

In the NWA simulation, there is significant star formation; all the most-massive substructures and the central halo have bound stars. This recovers the familiar 'overcooling problem', which we discuss further in Section 4.3. There is very little gas left over and the gas density is two orders of magnitude lower than in all other cases. In contrast, the NWB, WWA and WWB simulations are similar: there is very little star formation and significant remaining gas. The remaining gas shows bubble-like regions with overdensities of a factor of ~20. These overdensities are caused by heating from the star-forming regions. In the case of the WWA model, this is a result of the SN-driven galactic winds; for the NWB model, it is the result of heating from the SN feedback.

The key point to take away from Fig. 2 is that all the simulations with feedback produce qualitatively similar results: suppressed and spatially extended star formation. In particular, the NWB and WWA simulations are almost identical in every respect despite their quite different star formation and feedback mechanisms. For this reason, we plot only the results for the NWB simulation from hereon. We come to why the NWB and WWA simulations are so similar in Section 4.3. None of the simulations results in a significant 'blow-out' of gas, even in the galactic wind models. This is to be expected from the analytic arguments given in Section 2.

Recall that we used identical initial phase-space conditions for each of the simulations. We plot identical haloes which differ only in their star formation and feedback prescriptions. Yet the evolution of substructure in each of the simulations is quite different. The dark matter halo in the NWA simulation is much more centrally concentrated. This is a result of the increased merging due to the condensation of a large mass fraction of baryons at the centre of each substructure halo. In contrast, the WWA and NWB simulations are much less concentrated, corresponding to less merging. Finally, the WWB simulation (which has the strongest feedback – a combination of SN heating and galactic winds) shows the least merging of all. Substructure can still clearly be seen at the bottom left-hand side of the main halo, both in the dark matter and gas distributions, and at the bottom right-hand side in the dark matter.

The dissipation and collapse of gas significantly alters the merger history of haloes (cf. Macciò et al. 2006). However, it does not alter the dark matter density profiles, just the concentration. In Fig. 3, we plot the dark matter density profiles for the most-massive halo in the NWA, NWB and WWB simulations. Overplotted is the density profile of the most-massive halo in the dark matter only simulation (thick black line), and a theoretical prediction for how this profile would respond to the adiabatic contraction of the baryons in the NWA simulation (thick dashed line). For this analytic calculation, we used the usual prescription given in Blumenthal et al. (1986). This assumes that the halo collapses spherically without shell-crossing, conserving mass and specific angular momentum and with all halo particles moving on circular orbits. It provides a reasonable fit in the central regions to the NWA simulation, but performs poorly over intermediate radii. This is a known result. Even before the Blumenthal paper, Young (1980) demonstrated analytically that the assumption that the halo particles move on circular orbits leads to an overestimation of the contraction. More recently, Gnedin et al. (2004) have used simulations to demonstrate the same disparity on galaxy cluster scales. Here, we verify that the problem persists on the
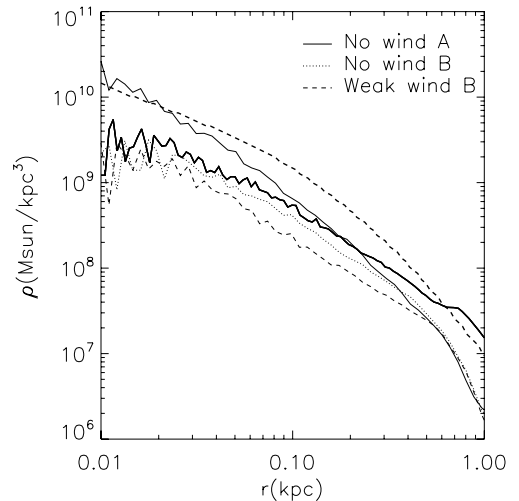

Figure 3. Dark matter density profiles for the most-massive halo in the NWA, NWB and WWB simulations. Overplotted is the density profile of the most-massive halo in the dark matter only simulation (thick black line), and a theoretical prediction for how this profile would respond to the adiabatic contraction of the baryons in the NWA simulation (thick dashed line).

scale of dwarf galaxies. The standard adiabatic contraction model should be used with caution on these scales. With SN feedback, there is a *lower* central halo density than that in the dark matter only run, while without feedback, the Blumenthal model overpredicts the effect. This agrees well with previous findings in the literature (Gnedin & Zhao 2002; Read & Gilmore 2005). All the dark matter haloes are well fitted by NFW profiles (Navarro, Frenk & White 1996); the typical concentration parameter and mass are $c \sim 4$, $M \sim 10^8 \, \mathrm{M_\odot}$. Even in the presence of a strong wind, a central dark matter cusp persists.

4.2 Stars viewed in projection

Fig. 4 shows the projected surface density (top panel) and velocity dispersion (bottom panel) for the stars in the two most-massive haloes (solid, dotted and dashed lines) in the NWA, NWB and WWB simulations. The thick and thin lines show two different projection angles. Overplotted are data from two LG dSphs which bracket the observed range of brightness: Draco (crosses) and, the recently discovered, Ursa Major (squares). The data were taken from Kleyna et al. (2001), Wilkinson et al. (2004), Willman et al. (2005) and Kleyna et al. (2005). Ursa Major is so faint that it has only one data point for the kinematics, but this suggests a very similar central velocity dispersion to Draco, despite it being an order of magnitude fainter. For Ursa Major's surface brightness distribution, we use the measured value for the scalelength and central brightness, but assume the same distribution as in Draco – hence the lack of error bars for these points.

In the NWA simulation, a significant amount of substructure within the main halo forms stars (see Fig. 2). This can clearly be seen in the surface density and projected velocity dispersion of the stars, both of which, for the second most-massive halo, show a significant bump correlated with the position of the largest substructure halo. In contrast, the NWB simulation, in which the substructure haloes form few or no stars, shows no such features. Such substructure is interesting. Several of the LG dwarfs appear to have bumps and wiggles in their projected velocity dispersion profiles. For two, the projected velocity dispersion appears to fall sharply towards the
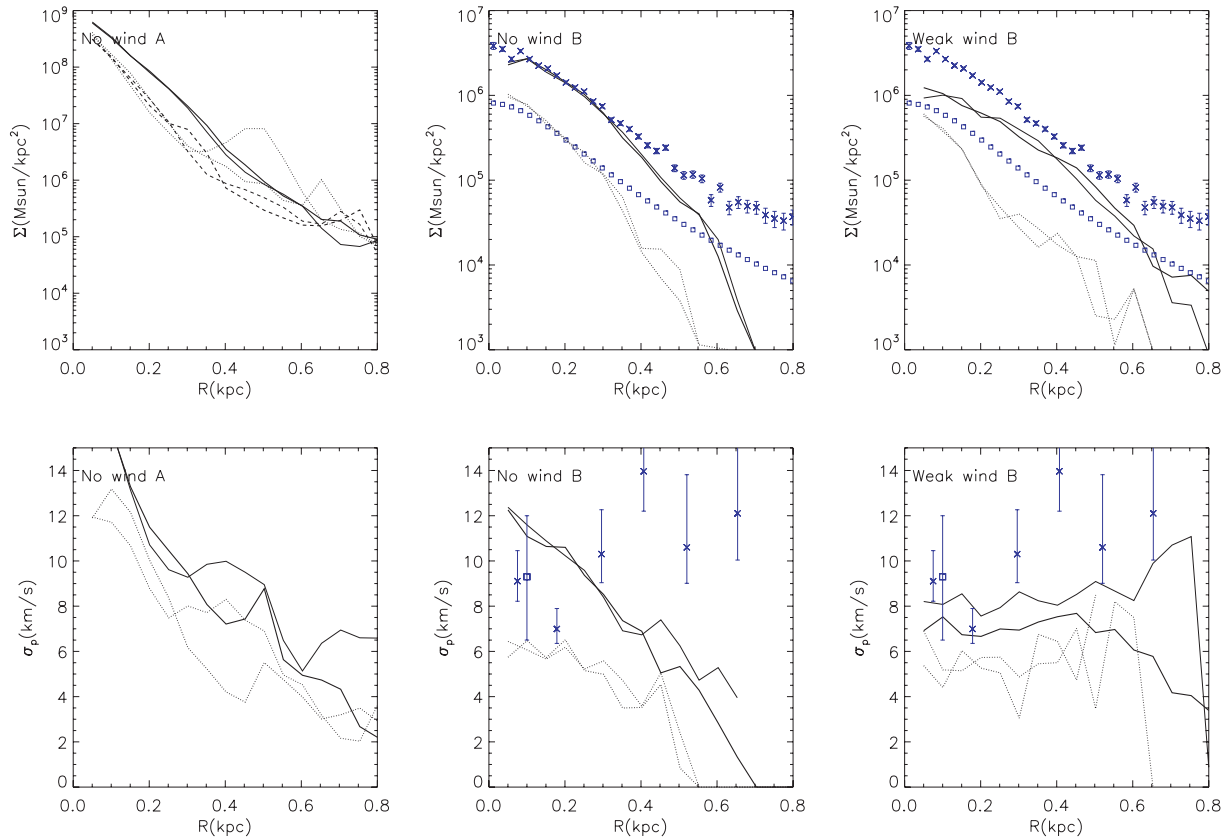
Figure 4. Projected surface density (top panel) and velocity dispersion (bottom panel) for stars in the two most-massive haloes (solid and dotted lines) in the NWA, NWB and WWB simulations. The thick and thin lines show two different projection angles which bracket the range of projected profiles. Overplotted are data from two LG dSphs which bracket the observed range of brightness: Draco (crosses) and, the recently discovered, Ursa Major (squares). The data were taken from Kleyna et al. (2001), Wilkinson et al. (2004), Willman et al. (2005) and Kleyna et al. (2005). Ursa Major is so faint that it has only one data point for the kinematics, but this suggests a very similar central velocity dispersion to Draco, despite it being an order of magnitude fainter. For Ursa Major's surface brightness distribution, we use the measured value for the scalelength and central brightness, but assume the same distribution as in Draco – hence, the lack of error bars for these points. Note that the data are from dSphs at redshift $z = 0$, while the simulations stop at $z = 10$. The comparison is only meaningful because the dSph stellar populations are old (see start of this section for further details).

edge of the light, which is dropping off smoothly (Wilkinson et al. 2004). For the WWA simulation, we did find one halo which retained a few stars within a subhalo. This can be seen in Fig. 2: note for the stars in the WWA simulation, there is an overdensity to the bottom left-hand side correlated with a dark matter subhalo. These subhalo stars also lead to a sharp drop in the projected velocity dispersion along some lines of sight, with no associated sharp truncation in the stellar surface density.

Such substructures are unlikely to be very long lived. However, it is interesting to speculate that kinematic bumps and wiggles could correspond to *late-infalling* substructure within the dwarfs.

The NWA simulation haloes have very high stellar surface densities and consistently falling projected velocity dispersions, whereas the LG dSphs have low surface densities and flat projected velocity dispersions (see data points, middle panels). This highlights the importance of SN heating and galactic winds for keeping the surface density of the stars low and producing galaxies which qualitatively resemble the dSphs of the LG.

The NWB halo much more closely resembles the LG dwarfs in their stellar distribution (see middle panels). The agreement inside ~400 pc is very encouraging, especially given that we have made no attempt to fine-tune our model to fit the data. However, for our simulated galaxies, the projected surface brightness and velocity dispersion both fall too steeply beyond ~400 pc.

The WWB model – which includes both SN heating and galactic winds – seems to solve these problems. The stars are more extended and the velocity dispersions are flat. This is exactly what we expect from gas mass loss. For the NWB simulation, the gas contributes significantly to the potential from ~0.4 kpc outwards. This explains why the stellar velocity dispersion is falling rather than flat (as would be expected if only the dark matter halo contributed to the potential). As shown in Read & Gilmore (2005) (and see also Mashchenko, Couchman & Sills 2005) gas mass loss will cause the remaining stars to expand and settle into an approximately exponential distribution – similar to that observed in Draco. Since the final potential is then dominated by the dark matter, the resulting velocity dispersions are flat.

However, it is important to remember that we are comparing galaxies forming at $z = 10$ with those observed at $z = 0$ in the LG. As such, the above discrepancies could also be the natural result of *external* feedback which is not included in our model. The tidal field from a large nearby galaxy, like the MW, will heat stars beyond a characteristic 'tidal radius' (r_t), leading to more extended surface brightness profiles and flat or rising projected velocity dispersions beyond r_t (Read et al. 2006a). Using the analytic formulae for r_t given in Read et al. (2006b), we find for a Draco of total mass $10^8 \, M_\odot$, with a tidal radius of $r_t = 400$ pc, that its orbital pericentre is ~20 kpc. This is consistent with measurements of the proper
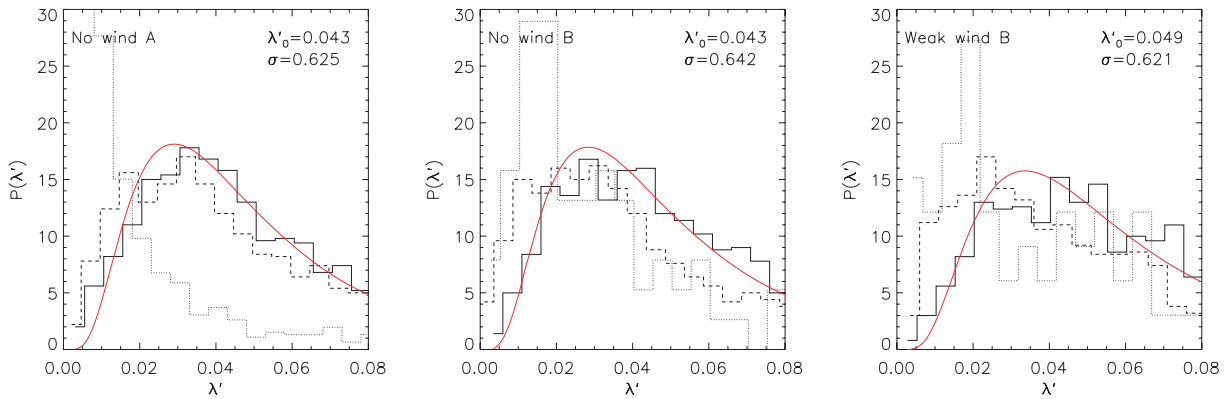
Figure 5. Distribution of spin parameters (λ') for the NWA, NWB and WWB simulations. The solid, dotted and dashed histograms show λ' for the dark matter, stars and gas, respectively. The smooth solid line is a lognormal fit to the dark matter λ' (see equation 8). The best-fitting parameters are marked on each plot.

motion of Draco (Kleyna et al. 2001). An alternative possibility is gas mass loss due to ram pressure stripping, which is likely to mimic the effect of the galactic wind in WWB. We return to these issues in Section 4.5.

4.3 Angular momentum and star formation

The angular momentum of a halo is typically parametrized by the dimensionless spin parameter given by (Bullock et al. 2001):

$$\lambda'_i = \frac{J_i}{\sqrt{2}M_i V_{\mathrm{vir}} R_{\mathrm{vir}}} \tag{6}$$

$$J_i = \left| \sum_{j=0}^{N} m_{i,j}\, \boldsymbol{r}_j \times \boldsymbol{v}_j \right|, \tag{7}$$

where the subscript, i, denotes the particle species (dark matter, stars or gas), J_i is the total angular momentum in that species, R_{vir} is the virial radius,[7] M_i is the mass of that species interior to R_{vir} and $V_{\mathrm{vir}} = \sqrt{GM_{\mathrm{vir}}/R_{\mathrm{vir}}}$ is the circular speed at the virial radius. This definition means that $\lambda'_i = 1/\sqrt{2}$ if all the particles are orbiting on circular orbits at R_{vir}.

Bullock et al. (2001) demonstrated that the lognormal profile provides an excellent fit to the distribution of spin parameters in their simulations. Colín et al. (2004) showed that the same form provides an excellent fit to dwarf galaxy scale haloes. The lognormal profile is given by

$$P(\lambda') = \frac{1}{\lambda'\sqrt{2\pi}\sigma} \exp\left[-\frac{\ln^2(\lambda'/\lambda'_0)}{2\sigma^2}\right]. \tag{8}$$

In Fig. 5, we plot the distribution of spin parameters (λ') for the NWA, NWB and WWB simulations. The solid, dotted and dashed histograms are for the dark matter, stars and gas, respectively. The smooth solid line shows the lognormal fit to the dark matter; the best-fitting parameters are shown at the top right-hand side of each plot. These are in excellent agreement with those found by Colín et al. (2004). In each case, we used all haloes with more than $\sim$10

---

[7] The virial radius is here defined as the radius within which the mean density of the halo is equal to 200 times the critical density of the universe at $z = 10$.

particles (in dark matter, stars and gas, respectively), which is about $\sim$1000 haloes per simulation.

For the NWA simulation, we recover the well-known overcooling problem. The simple star formation prescription we use turns all the cold gas into stars and overmerging leads to a very low final stellar angular momentum. The NWB simulation alleviates this problem, but low angular momentum stars still remain. The WWB simulation, with the strongest feedback, prevents almost any angular momentum loss from the stars. As expected analytically (see e.g. Maller & Dekel 2002), feedback solves the overcooling problem by preventing the subhaloes from efficiently forming stars. However, we should be a little cautious. Kaufmann et al. (2006) have recently shown that, for *disc galaxies*, greater than 10^6 particles are required *per galaxy* for angular momentum loss due to spurious numerical transport to be at an acceptable level. Even with our very high resolution, our best resolved haloes have $O(10^5)$ particles – an order of magnitude too low to avoid such numerical overcooling. The angular momentum loss mechanisms identified by Kaufmann et al. (2006) are: viscous friction between the cold disc and hot halo; transfer between the spiral arms and bar of the disc and the dark matter halo; and angular momentum loss from infalling cold gas clouds. In our simulations, none of these mechanisms can act. In the simulation without SN feedback (NWA), all subhaloes turn their gas into stars. In this case, discs do not form because of angular momentum loss in mergers. With SN feedback (NWB, WWA, WWB, SWA), we prevent stars from forming in the smaller subhaloes. Now discs do not form because the velocity dispersion in the gas, maintained by the feedback at $\sim$10 km s^{-1}, is comparable to the rotational velocity. It is essentially a disc with a very large scale height. We can see this in Fig. 5, where, in all of the simulations with SN feedback, the stars and gas retain their initial angular momentum, but do not significantly condense. For these simulations, with SN feedback, stars form stochastically where the density fluctuates upwards. It is likely that such fluctuations are imprinted by numerical noise, but they can be thought of as physical. In the 'real' universe, such fluctuations are likely to exist as a result of external tides and internal microphysics.

The above explains why the feedback recipe is not critical in determining the final morphology of the galaxy. Provided that it prevents the subhaloes from efficiently forming stars then it will work. Galactic winds do this by ejecting a proportion of the gas available for star formation; feedback from SN heating does this by heating locally cold gas which would otherwise form stars. This is a known result. For example, in Eke, Efstathiou & Wright (2000),

they showed that the overcooling problem can be solved by simply delaying star formation until most subhaloes have merged into the main galaxy.

Finally, note that while in the NWB and WWB simulations the stars retain significant angular momentum with $\lambda'_0 \sim 0.05$, this would be very hard to detect in practice. None of the galaxies shows measurable tip-to-tip rotation of greater than $\sim 2 \,\mathrm{km\,s^{-1}}$. This is because the stars remain extended and do not collapse and 'spin up'.

4.4 Metallicities

In Fig. 6, we plot the metallicity distributions of the three most-massive haloes in the WWB simulation (solid, dotted and dashed histograms); the NWB simulation showed very similar results (recall that the simple star formation prescription – A – does not produce reliable metallicity output). The smooth solid lines show data for the LG dSphs taken from Mateo (1998). We have assumed that these distributions are Gaussian, although detailed recent observations suggest that more complex distributions are likely (see e.g. Tolstoy et al. 2004; Koch et al. 2006).

Recall from Section 3 that the absolute value of the metallicity for our haloes should be taken with caution as we have chosen a yield which produces a good fit to the metallicity of the IGM at $z = 3$ (Theuns et al. 2002). It is not clear that this is the relevant value for our dwarf galaxies forming at $z = 10$. That caveat aside, our metallicities are systematically lower than those of the observed dwarfs. This is, perhaps, to be expected: the galaxies we form in WWB seem to be less massive, both in stars and dynamically, than most observed nearby dwarfs (see Figs 4 and 7 in the following section). Recent observations of the *faintest* and lowest-mass dwarf galaxies suggest metallicities which are lower than the mean of those shown in Fig. 6. The faintest galaxy to date – Bootes – has a mean metallicity of ~ -2.5 (Munoz et al. 2006), closer to the most-massive galaxy we form in WWB (especially considering that the yield is so poorly constrained).

Figure 7. Total stellar mass as a function of dark matter mass within the virial radius for the 10 most-massive haloes in the NWA, NWB, WWA, WWB and SWA simulations. Overplotted are data for the LG dwarfs and nearby dIrrs. See the text for details of the data compilation.

The spread, which is more certain in our models, appears to match quite well that of the nearby dwarfs. However, in our models it is clearly non-Gaussian (recall that we assumed Gaussianity for the data). The shape of our distribution matches very well that of more detailed modelling recently performed by Marcolini et al. (2006). We find, similar to their results, an asymmetric distribution peaked at high metallicity, with a tail to lower metallicities. Recent work by Bellazzini et al. (2002) suggests such asymmetries may be present in the Draco and UMi dSphs, but it would be interesting to confirm this as a generic feature in future observational works.

Our model may provide a simple solution to the 'abundance problem' for the LG dwarfs. Tolstoy et al. (2003) found, from detailed spectroscopy of resolved stars, that: (i) the abundance[8] of stars in four LG dSphs is lower than that observed in the old stars of the MW stellar halo; and (ii) the mean metallicity of the MW halo stars is much lower than that of the dwarfs: $\langle[\mathrm{Fe/H}]\rangle \sim -3$. This presents a puzzle since it suggests that the MW stellar halo cannot have formed from galaxies like the LG dSphs seen at the present epoch. In our model this is not a problem. Our progenitor 'BBBs' do have the correct mean metallicity. Furthermore, while we do not explicitly track abundances in our code, we can expect their abundances to be high. This is because there is a link between abundance and the star formation time-scale. Stars which form rapidly are only enriched by Type II supernovae which do not produce much iron; stars which form more slowly can be enriched by Type Ia supernovae which produce more iron relative to other metals and therefore lower the abundance (see e.g. Binney & Merrifield 1998). Our early-forming BBBs form stars rapidly and are likely to be of high abundance. Over a Hubble time, as our BBBs gradually form more stars, they then lower their abundance and start to look more like the LG dSphs. This agrees well with earlier studies in the literature (Bullock & Johnston 2005; Robertson et al. 2005; Font et al. 2006).
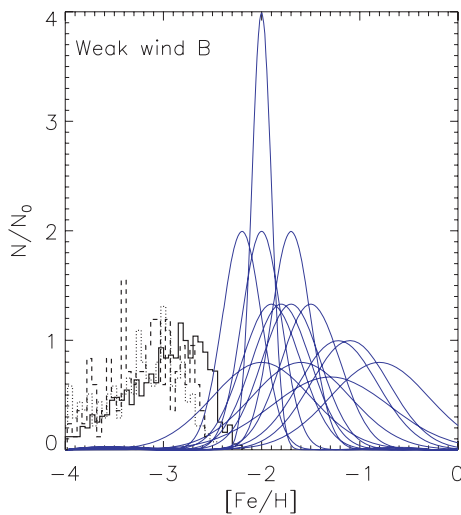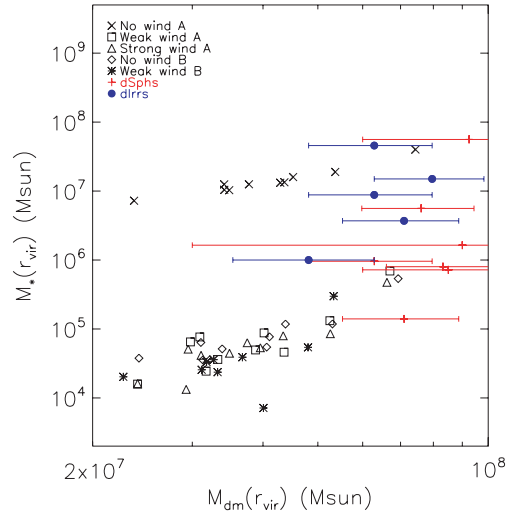

Figure 6. Metallicity distributions of the three most-massive haloes in the WWB simulation (thick solid, dotted and dashed histograms). The smooth solid lines show data for the LG dSphs taken from Mateo (1998). We have assumed that these distributions are Gaussian, although detailed recent observations suggest that more complex distributions are likely (see e.g. Tolstoy et al. 2004; Koch et al. 2006).

---

[8] The abundance is the mass of a given 'metal' (element heavier than Helium) relative to iron.

4.5 Mass-to-light ratios

In Fig. 7, we plot the total stellar mass as a function of dark matter mass within the virial radius for the 10 most-massive haloes in the NWA, NWB, WWA, WWB and SWA simulations. We stop at the first 10 haloes since the smallest of these haloes have only 10^4 M$_\odot$ in stars which corresponds to just ∼10 star particles. Overplotted are data for the LG dwarfs and nearby dIrrs.

It is difficult to obtain an accurate compilation for nearby dwarf galaxies. The dIrrs have only gas kinematic measurements from which the dynamical mass can be derived, while the dSphs have only stellar kinematics (since they are devoid of gas). A further complication comes from the quality of the older versus the newer data. Some of the dSphs now have excellent data (like that over-plotted in Fig. 4). However, most have older data which were typically taken only near the centre of the galaxy. It is now known that these older measurements systematically underestimate the mass of the dSphs. Our adopted solution is to use only the latest data. These have been compiled from Begum & Chengalur (2004, 2003), Begum et al. (2006), Kleyna et al. (2005), Willman et al. (2005), Muñoz et al. (2005), Kleyna et al. (2004), Wilkinson et al. (2004), Kleyna et al. (2001), Walker et al. (2005, 2006), Irwin & Hatzidimitriou (1995) and Westfall et al. (2006). For the dSphs, we plot the masses derived from detailed mass modelling in all cases except for Ursa Major (the faintest dSph).[9] For this dSph and for the dIrrs we assume an isotropic isothermal sphere model. This gives

$$M(r) = \frac{3f\overline{\sigma_p^2}r}{G},\qquad(9)$$

where G is the gravitational constant, $\overline{\sigma_p^2}$ the measured *mean projected* velocity dispersion squared, $r = 1$ kpc $\sim R_{vir}$ is the radius enclosing the mass and f is a small correction factor. $f = 1.4$ is chosen such that we would recover the correct mass for the Draco dSph (obtained from detailed distribution function modelling) using equation (9).

There are two key things to take away from Fig. 7. First, note how rapidly the stellar mass falls as the halo mass is reduced in all the simulations with internal feedback from SNe. The details of the star formation and feedback recipes are not important for determining the final stellar masses. In all cases, the stellar mass falls two orders of magnitude for a decrease in halo mass of little over 30 per cent. This was expected from the analytic arguments presented in Section 2. Secondly, note that the LG dwarfs and nearby dIrrs seem to show a cut-off in their dynamical mass at ∼5 × 10^7 M$_\odot$, but a wide range in stellar masses. The data are well bracketed by our NWA and other simulations.

The dSphs are consistent with our most-massive haloes with all the gas removed; while the dIrrs lie close to the NWA model suggesting that, over a Hubble time, they have managed to turn most of their initial gas into stars. The fact that this process is a slow one is important. First, because star formation is inefficient, it allows gas to be slowly removed. Ram pressure stripping is one such mechanism which could achieve this (see e.g. Mayer et al. 2005). It has the advantage that galaxies which lie close to the MW or M31 will be more rapidly stripped than those which lie further away, naturally reproducing the distance–morphology relation (see Section 1).

---

[9]Ursa Major has only one velocity dispersion measurement. It could be reasonably argued that this makes it as unreliable as the older data. However, unlike the older data, this one data point lies ∼250 pc away from the centre of the galaxy. This makes it more likely to be representative of the mean velocity dispersion than older measurements.

Secondly, recall that in the NWA simulation, the stellar density was much higher than that observed in the LG dwarfs and too much substructure formed stars. This occurred because the star formation in the NWA simulation was too efficient. Even for the most-isolated dIrr which eventually turns all its gas into stars, SN feedback and reionization have a role to play in keeping the star formation efficiency low and spatially extended. This prevents substructure forming stars and keeps the stellar surface density and rotational velocity low, consistent with observations.

One caveat is worth mentioning. In all cases, it is our most-massive simulated galaxies which resemble the *least-massive* LG dSphs. For the WWB simulation, none of our simulated galaxies achieves enough stellar mass to be consistent with observations (this can also be seen in Fig. 4). This suggests that either our feedback prescription is too strong, or the observed dwarfs formed from the merger of several of our BBBs, with some continued star formation over a Hubble time. It is not possible to address which of these is correct without running larger-box simulations of comparable resolution and continuing down to lower redshift. We leave this for future work.

5 DISCUSSION

5.1 A connection to galaxies in clusters?

Trentham & Hodgkin (2002) have recently discovered a new class of very low surface brightness (VLSB) galaxies in the Virgo cluster. These galaxies are extremely faint, spheroidal in morphology and extended over several kpc. So far in this paper, we have talked only about the low-density environment of the LG. In clusters, the picture could be quite different. While little is known about these VLSB galaxies and follow-up observations are currently underway, an intriguing possibility is that these too are naked stellar haloes. Like the dSphs of the LG, they may have lost their gas faster than they could turn it into stars, leaving them with just the extended, low rotational velocity, metal-poor, old stellar halo component. If true, further observations should confirm that these VLSB galaxies have all the properties of old stellar haloes. They are likely more massive than their LG cousins, however.

5.2 The formation of globular clusters

We have presented the case for a 'BBB' for galaxy formation. These gas-rich building blocks have total mass $M_{crit} \sim 10^8$ M$_\odot$ and form ∼10^6 M$_\odot$ in stars before reionization. However, we can see in the universe that stars form on smaller scales than this in star clusters and globular clusters. In part this is a natural result of fragmentation: in our model, these star clusters and globular clusters form *within* such BBBs. However, the picture cannot be quite this simple for two reasons. First, we require that the phase-space density of stars in our building blocks is low, yet in globular clusters and massive star clusters it is very high. Secondly, we have outlined the importance of SN winds in suppressing star formation on mass scales $\lesssim 10^8$ M$_\odot$. How then can star clusters with stellar mass $\lesssim 10^5$ M$_\odot$ ever form?

Kroupa & Boily (2002) provided some plausible answers to these problems. On the scale of star clusters, the star formation time-scales are shorter than the lifetime of a typical O-star. This explains why gas expulsion from SNe is not likely to be of great importance for star cluster formation (though it becomes very important for driving galactic scale winds and heating surrounding gas, as we have shown here). Instead, stellar winds and ionizing flux from O-stars are the

most important forms of internal feedback for star clusters forming with masses $\lesssim 10^4$ M$_\odot$. Above 10^4 M$_\odot$, SNe become important for star clusters and can allow them to self-enrich. Such massive clusters are still protected from destruction by SN winds, however, by their high density (Morgan & Lake 1989).

It is not clear how the very high gas densities required to form globular clusters can be achieved. Observational evidence suggests a link to the star formation rate. In interacting systems (like galaxy mergers) and strong starbursts, the globular cluster and massive star cluster formation rates are much larger than in more quiescent systems (Whitmore et al. 1993; Zepf & Ashman 1993). This view is also supported by recent theoretical work (see e.g. Li, Mac Low & Klessen 2004). It is clear that accurately modelling such effects is beyond the scope of this work.

6 CONCLUSIONS

Using analytic arguments and a suite of very high resolution ($\sim 10^3$ M$_\odot$ per particle) cosmological hydrodynamical simulations, we have argued that high-redshift, $z \sim 10$, $M \sim 10^8$ M$_\odot$, haloes, form the smallest 'BBB' for galaxy formation. These haloes are just massive enough to efficiently form stars through atomic line cooling and to hold on to their gas in the presence of SN winds and reionization. These combined effects, in particular that of the SN feedback, create a sharp transition: over the mass range $3\text{--}10 \times 10^7$ M$_\odot$, the BBBs drop two orders of magnitude in stellar mass. Below $\sim 2 \times 10^7$ M$_\odot$, galaxies will be dark with almost no stars and no gas. Above this scale is the smallest unit of galaxy formation: the BBB.

We have shown that SN feedback is important for these smallest galaxies, not because it ejects the gas, but because it keeps the gas hot and extended. We find that the details of such feedback are not critical. Whether implemented as a heating term for gas surrounding star-forming regions, or as a galaxy-wide wind, the results are similar. However, the combination of SN heating *and* SN-driven galactic winds gives the best agreement with observations. Such feedback works by reducing the star formation efficiency in subhaloes. This keeps the surface density and rotational velocity of the stars which do form low. The smallest observed galaxies in the LG have very low surface brightness, as does the MW old stellar halo. Without such SN feedback our model cannot reproduce these properties. Efficient cooling of the SN ejecta is prevented by the ionizing background from reionization.

We connected these BBBs to galaxies observed at $z = 0$ using a mixture of linear theory arguments and results from other studies in the literature. In a galaxy the size of the MW, O(100), such building blocks will be accreted. Moore et al. (2006) have recently shown that, of these, ~ 10 per cent survive to form the lowest-mass LG dwarf galaxies. The remainder form the bulk of the MW old stellar halo. The survivors will slowly form stars and lose gas over a Hubble time. Since neither reionization nor SN winds actually eject gas from these galaxies, we require some other mechanism for this. Ram pressure stripping is a likely candidate. In this case, those BBBs on benign orbits which keep them far away from the MW or Andromeda manage to retain their gas and slowly form stars – these become the lowest-mass dIrrs; those on more severe orbits lose their gas faster than they can form stars and become the dwarf spheroidals (dSphs). Both galaxy types become more metal rich and of lower abundance than the progenitor building blocks due to their more extended star formation. In this picture, the dSphs are 'naked stellar haloes', while the dIrrs have both an old, metal-poor, stellar halo and a younger, more centrally concentrated population of stars. There is increasing observational evidence that this is indeed the case (Minniti & Zijlstra 1996; Minniti et al. 2003; Aparicio et al. 2000).

We have shown that the stars in our high-redshift BBBs resemble with those in the faintest dSphs in the LG at the present epoch. This does not prove, however, that all the LG dSphs formed in this way. Kravtsov et al. (2004) and Mayer et al. (2005) have suggested that some formed from quite different mechanisms and were much more massive in the past than at present.

There should be many galaxies in the LG with surface brightness an order or two orders of magnitude fainter than those already found. We predict that these galaxies will have very similar total mass ($2\text{--}10 \times 10^7$ M$_\odot$) to those satellites already discovered.

Finally, we have commented almost exclusively on the low-density LG, rather than the high-density cluster environment. This is mainly because the BBBs we form in our simulations are so small and faint that, at the moment, we can only hope to observe their $z = 0$ counterparts in the very nearby universe. We expect, however, many such BBBs to survive to the present epoch, even in cluster environments. The continued accretion of such BBBs over a Hubble time should lead to an old metal-poor stellar halo being a ubiquitous feature of all large galaxies. However, it is important not to think of these BBBs as *the* building block for galaxy formation. We stress that they are the *smallest* building blocks and the major contributors to old stellar haloes, not the bricks from which all galaxies are made.

REFERENCES

Abel T., Anninos P., Norman M. L., Zhang Y., 1998, ApJ, 508, 518
Adelberger K. L., Steidel C. C., Shapley A. E., Pettini M., 2003, ApJ, 584, 45
Adelberger K. L., Shapley A. E., Steidel C. C., Pettini M., Erb D. K., Reddy N. A., 2005, ApJ, 629, 636
Aparicio A., Tikhonov N., Karachentsev I., 2000, AJ, 119, 177
Avila-Reese V., Colín P., Valenzuela O., D'Onghia E., Firmani C., 2001, ApJ, 559, 516
Barkana R., Loeb A., 1999, ApJ, 523, 54
Begum A., Chengalur J. N., 2003, A&A, 409, 879
Begum A., Chengalur J. N., 2004, A&A, 413, 525
Begum A., Chengalur J. N., Karachentsev I. D., Kaisin S. S., Sharina M. E., 2006, MNRAS, 365, 1220
Bellazzini M., Ferraro F. R., Origlia L., Pancino E., Monaco L., Oliva E., 2002, AJ, 124, 3222
Benson A. J., Frenk C. S., Lacey C. G., Baugh C. M., Cole S., 2002, MNRAS, 333, 177
Binney J., Merrifield M., 1998, Galactic Astronomy. Princeton Univ. Press, Princeton, NJ
Blumenthal G. R., Faber S. M., Flores R., Primack J. R., 1986, ApJ, 301, 27
Bode P., Ostriker J. P., Turok N., 2001, ApJ, 556, 93
Bullock J. S., Dekel A., Kolatt T. S., Kravtsov A. V., Klypin A. A., Porciani C., Primack J. R., 2001a, ApJ, 555, 240

Bullock J. S., Kravtsov A. V., Weinberg D. H., 2001b, ApJ, 548, 33
Bullock J. S., Johnston K. V., 2005, ApJ, 635, 931
Bullock J. S., Kravtsov A. V., Weinberg D. H., 2000, ApJ, 539, 517
Bunker A., Stanway E., Ellis R., McMahon R., Eyles L., Lacy M., 2006, New Astron. Rev., 50, 94
Colín P., Klypin A., Valenzuela O., Gottlöber S., 2004, ApJ, 612, 50
Dekel A., Silk J., 1986, ApJ, 303, 39
Dekel A., Woo J., 2003, MNRAS, 344, 1131
Desjacques V., Nusser A., Haehnelt M. G., Stoehr F., 2004, MNRAS, 350, 879
Dolphin A. E., 2002, MNRAS, 332, 91
D'Onghia E., Lake G., 2004, ApJ, 612, 628
Efstathiou G., 2000, MNRAS, 317, 697
Eggen O. J., Lynden-Bell D., Sandage A. R., 1962, ApJ, 136, 748
Eisenstein D. J., Hu W., 1999, ApJ, 511, 5
Eke V., Efstathiou G., Wright L., 2000, MNRAS, 315, L18
Fan X. et al., 2005, AJ, 132, 117
Font A. S., Johnston K. V., Bullock J. S., Robertson B. E., 2006, ApJ, 638, 585
Gnedin O. Y., Kravtsov A. V., Klypin A. A., Nagai D., 2004, ApJ, 616, 16
Gnedin N. Y., Kravtsov A. V., 2006, ApJ, 645, 1054
Gnedin O. Y., Zhao H., 2002, MNRAS, 333, 299
Haardt F., Madau P., 1996, ApJ, 461, 20
Hayashi E., Navarro J. F., Taylor J. E., Stadel J., Quinn T., 2003, ApJ, 584, 541
Hernandez X., Gilmore G., Valls-Gabaud D., 2000, MNRAS, 317, 831
Hoyle F., 1953, ApJ, 118, 513
Irwin M., Hatzidimitriou D., 1995, MNRAS, 277, 1354
Katz N., Weinberg D. H., Hernquist L., 1996, ApJS, 105, 19
Kauffmann G., White S. D. M., Guiderdoni B., 1993, MNRAS, 264, 201
Kaufmann T., Mayer L., Wadsley J., Stadel J., Moore B., 2006, preprint (astro-ph/0601115)
Kawata D., Arimoto N., Cen R., Gibson B. K., 2005, ApJ, 641, 785
Kazantzidis S., Mayer L., Mastropietro C., Diemand J., Stadel J., Moore B., 2004, ApJ, 608, 663
Kennicutt R. C., 1989, ApJ, 344, 685
Kleyna J. T., Wilkinson M. I., Evans N. W., Gilmore G., 2001, ApJ, 563, L115
Kleyna J. T., Wilkinson M. I., Evans N. W., Gilmore G., 2004, MNRAS, 354, L66
Kleyna J. T., Wilkinson M. I., Evans N. W., Gilmore G., 2005, ApJ, 630, L141
Klypin A., Kravtsov A. V., Valenzuela O., Prada F., 1999, ApJ, 522, 82
Koch A., Grebel E. K., Wyse R. F. G., Kleyna J. T., Wilkinson M. I., Harbeck D. R., Gilmore G. F., Evans N. W., 2006, AJ, 131, 895
Kravtsov A. V., Gnedin O. Y., Klypin A. A., 2004, ApJ, 609, 482
Kroupa P., Boily C. M., 2002, MNRAS, 336, 1188
Lacey C., Cole S., 1993, MNRAS, 262, 627
Larson R. B., 1974, MNRAS, 169, 229
Le Bourlot J., Pineau des Forêts G., Flower D. R., 1999, MNRAS, 305, 802
Li Y., Mac Low M.-M., Klessen R. S., 2004, ApJ, 614, L29
Mac Low M., Ferrara A., 1999, ApJ, 513, 142
Macciò A. V., Moore B., Stadel J., Diemand J., 2006, MNRAS, 366, 1529
Maller A. H., Dekel A., 2002, MNRAS, 335, 487
Marcolini A., D'Ercole A., Brighenti F., 2006, MNRAS, (doi: 10.1111/j.1365-2966.2006.10671.x)
Martin C. L., 1999, ApJ, 513, 156
Mashchenko S., Couchman H. M. P., Sills A., 2005, ApJ, 624, 726
Mateo M. L., 1998, ARA&A, 36, 435
Mayer L., Governato F., Colpi M., Moore B., Quinn T., Wadsley J., Stadel J., Lake G., 2001a, ApJ, 559, 754
Mayer L., Governato F., Colpi M., Moore B., Quinn T., Wadsley J., Stadel J., Lake G., 2001b, ApJ, 547, L123
Mayer L., Mastropietro C., Wadsley J., Stadel J., Moore B., 2005, MNRAS, 369, 1021
Minniti D., Zijlstra A. A., 1996, ApJ, 467, L13
Minniti D., Borissova J., Rejkuba M., Alves D. R., Cook K. H., Freeman K. C., 2003, Sci, 301, 1508
Moore B., Diemand J., Madau P., Zemp M., Stadel J., 2006, MNRAS, 368, 563
Morgan S., Lake G., 1989, ApJ, 339, 171
Muñoz R. R. et al., 2005, ApJ, 631, L137
Munoz R. R. et al., 2006, preprint (astro-ph/0606271)
Navarro J. F., Frenk C. S., White S. D. M., 1996, ApJ, 462, 563
Ott J., Walter F., Brinks E., 2005, MNRAS, 358, 1453
Peacock J. A., 1999, Cosmological Physics. Cambridge Univ. Press, Cambridge
Peebles P. J. E., 1984, ApJ, 277, 470
Peebles P. J. E., Dicke R. H., 1968, ApJ, 154, 891
Peel A. C., 2006, MNRAS, 365, 1191
Porciani C., Dekel A., Hoffman Y., 2002, MNRAS, 332, 325
Quinn T., Katz N., Efstathiou G., 1996, MNRAS, 278, L49
Rauch M., Becker G. D., Viel M., Sargent W. L. W., Smette A., Simcoe R. A., Barlow T. A., Haehnelt M. G., 2005, ApJ, 632, 58
Read J. I., Gilmore G., 2005, MNRAS, 356, 107
Read J. I., Wilkinson M. I., Evans N. W., Gilmore G., Kleyna J. T., 2006a, MNRAS, 367, 387
Read J. I., Wilkinson M. I., Evans N. W., Gilmore G., Kleyna J. T., 2006b, MNRAS, 366, 429
Ricotti M., Gnedin N. Y., 2005, ApJ, 629, 259
Robertson B., Bullock J. S., Font A. S., Johnston K. V., Hernquist L., 2005, ApJ, 632, 872
Searle L., Zinn R., 1978, ApJ, 225, 357
Seljak U. et al., 2005, Phys. Rev. D, 71, 103515
Seljak U., Slosar A., McDonald P., 2006, preprint (astro-ph/0604335)
Skillman E. D., 2005, New Astron. Rev., 49, 453
Springel V., 2005, MNRAS, 364, 1105
Springel V., Hernquist L., 2002, MNRAS, 333, 649
Springel V., Hernquist L., 2003, MNRAS, 339, 289
Springel V., Yoshida N., White S. D. M., 2001, New Astron., 6, 79
Spergel D. N. et al., 2003, ApJS, 148, 175
Spergel D. N. et al., 2006, preprint (astro-ph/0603449)
Stoehr F., White S. D. M., Tormen G., Springel V., 2002, MNRAS, 335, L84
Susa H., Umemura M., 2004, ApJ, 600, 1
Theuns T., Viel M., Kay S., Schaye J., Carswell R. F., Tzanavaris P., 2002, ApJ, 578, L5
Tolstoy E., Venn K. A., Shetrone M., Primas F., Hill V., Kaufer A., Szeifert T., 2003, AJ, 125, 707
Tolstoy E. et al., 2004, ApJ, 617, L119
Trentham N., Hodgkin S., 2002, MNRAS, 333, 423
Vaduvescu O., McCall M. L., Richer M. G., Fingerhut R. L., 2005, AJ, 130, 1593
Viel M., Haehnelt M. G., Lewis A., 2006, MNRAS, 370, L51
Viel M., Haehnelt M. G., Springel V., 2004, MNRAS, 354, 684
Walker M. G., Mateo M., Olszewski E. W., Bernstein R. A., Wang X., Woodroofe M., 2005, AJ, 131, 2114
Walker M. G., Mateo M., Olszewski E. W., Pal J. K., Sen B., Woodroofe M., 2006, ApJ, 642, L41
Westfall K. B., Majewski S. R., Ostheimer J. C., Frinchaboy P. M., Kunkel W. E., Patterson R. J., Link R., 2006, AJ, 131, 375
White S. D. M., Rees M. J., 1978, MNRAS, 183, 341
Whitmore B. C., Schweizer F., Leitherer C., Borne K., Robert C., 1993, AJ, 106, 1354
Wilkinson M. I., Evans N. W., 1999, MNRAS, 310, 645
Wilkinson M. I., Kleyna J. T., Evans N. W., Gilmore G. F., Irwin M. J., Grebel E. K., 2004, ApJ, 611, L21
Willman B. et al., 2005, ApJ, 626, L85
Wyithe S., Loeb A., 2006, Nat, 441, 322
Young P., 1980, ApJ, 242, 1232
Zepf S. E., Ashman K. M., 1993, MNRAS, 264, 611

This paper has been typeset from a TEX/LATEX file prepared by the author.